Light-Enhanced Spin Diffusion in Hybrid Perovskite Thin Films and Single Crystals

Feng Li,[†,‡] Junfeng Ding,[†,#] Weili Yu,[§] Xinwei Guan,[∥] Peng Wang,[⊥] Di Wu,[⊥] and Tom Wu[*,∥]

[†]Materials Science and Engineering, King Abdullah University of Science and Technology, Thuwal 23955-6900, Saudi Arabia
[‡]College of Physical Science and Technology, Sichuan University, Chengdu 610064, People's Republic of China
[§]Changchun Institute of Optics, Fine Mechanics and Physics, Chinese Academy of Sciences (CAS), Changchun 130033, People's Republic of China
[∥]School of Materials Science and Engineering, University of New South Wales (UNSW), Sydney, New South Wales 2052, Australia
[⊥]National Laboratory of Solid State Microstructures and Department of Physics, Nanjing University, 22 Hankou Road, Nanjing 210093, People's Republic of China

S *Supporting Information*

ABSTRACT: Organolead trihalide perovskites have attracted substantial interest with regard to applications in charge-based photovoltaic and optoelectronic devices because of their low processing costs and remarkable light absorption and charge transport properties. Although spin is an intrinsic quantum descriptor of a particle and spintronics has been a central research theme in condensed matter physics, few studies have explored the spin degree of freedom in the emerging hybrid perovskites. Here, we report the characterization of a spin valve that uses hybrid perovskite films as the spin-transporting medium between two ferromagnetic electrodes. Because of the light-responsive nature of the hybrid perovskite, a high magnetoresistance of 97% and a large spin-diffusion length of 81 nm were achieved at 10 K under light illumination in polycrystalline films. Furthermore, by using thin perovskite single crystals, we discovered that the spin-diffusion length was able to reach 1 μm at low temperatures. Our results indicate that the spin relaxation is not significant as previously expected in such lead-containing materials and demonstrate the potential of low-temperature-processed hybrid perovskites as new active materials in spintronic devices.

KEYWORDS: hybrid perovskites, spintronics, spin valve, magnetoresistance, spin-diffusion length

INTRODUCTION

Spin is a key quantum degree of freedom for elemental particles, and spintronics is based on the ability to store, transport, and manipulate the spin state of electrons in heterostructured devices. The discovery of giant magnetoresistance (GMR) and tunneling magnetoresistance (TMR) in spin valves has revolutionized magnetic recording and memory technologies.[1−3] At present, intense research efforts are being devoted to developing effective methods of generating and detecting spin-polarized carriers, and it is of paramount importance to identify new materials that can effectively retain spin polarization during charge transport.

Both inorganic and organic materials have been explored as spin transport media. Inorganic materials, such as high-purity elemental and compound semiconductors, possess high carrier mobility (μ).[4,5] Because the spin-diffusion length (λ_S) can be expressed as $\lambda_S = \sqrt{(k_B T/e)\mu t_S}$ (k_B: Boltzmann constant, T: temperature, and t_S: spin relaxation time),[6,7] a high μ is expected to lead to a large λ_S. Inorganic semiconductors are

often characterized by short t_S values; thus, they are not suitable for coherent spin manipulation.[6,7] Organic semiconductors (OSCs) possess several promising advances over their inorganic counterparts, such as flexibility, low cost, and versatility of chemical synthesis.[6−10] Furthermore, OSCs are mainly composed of atoms with a low atomic number, Z, thus leading to weak spin−orbit coupling (SOC) and hyperfine interaction (HFI) and consequently to extremely large t_S values.[8−10] However, OSCs exhibit somewhat short λ_S values because of the low μ (e.g., on the order of 10^{-6} to 10^{-5} cm^2 V^{-1} s^{-1} for the widely investigated OSC Alq$_3$),[6,7,9,10] thus severely decreasing the MR of organic devices. Therefore, to develop high-performance spintronic devices, exploring new candidates that combine the advantages of both organic and inorganic materials will be of great significance.
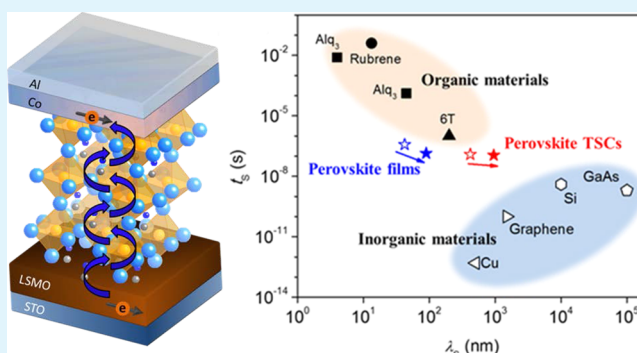
In recent years, methylammonium lead trihalide perovskites ($MAPbX_3$, where MA is CH_3NH_3 and X is Cl, Br, or I) have attracted significant interest for optoelectronic applications, such as photovoltaic cells,[11−14] light-emitting diodes/transistors,[15,16] lasers,[17] photodetectors,[18−20] phototransistors,[21−23] and laser cooling.[24] This emerging class of materials exhibits excellent properties, such as cost effectiveness, ease of processing, adjustable band gap, and large light absorption coefficients throughout the UV−vis region.[13,14] More importantly, this class of materials has also been reported to exhibit a balanced carrier mobility and long carrier diffusion length,[25,26] especially for hybrid perovskite single crystals,[27,28] thus suggesting the potential for a long λ_S and further promising applications in spintronics. There have been works exploring the magnetic field effects in $MAPbX_3$, and magneto-photoluminescence (PL) and polarized electroluminescence emission effects were demonstrated in perovskites.[29−32] In addition, the GMR response and the long spin lifetime and spin-diffusion length were reported in the vertical spin valves based on hybrid perovskite films.[31−33] However, an in-depth investigation of spin transport in hybrid perovskite spin valves, especially the single-crystal perovskites, has been lacking despite the highly promising potential of such hybrid perovskite materials in spintronic applications. Furthermore, the light manipulation effect on spin-dependent transport properties in spintronic devices made of various photoactive semiconductors has been widely investigated and has attracted intensive research interests.[34−36] Our prior results on hybrid perovskite phototransistors have demonstrated that light illumination is effective in increasing the carrier mobility and enhancing the charge transport in hybrid perovskites,[21] but the possible light modulation effect on the spin transport in such hybrid materials remains unexplored.

Here, we report the development of a novel spin valve based on hybrid perovskites and its carrier/spin injection and transport characteristics. An MR ratio greater than 97% was achieved at 10 K under illumination, which is quite high among the MR values reported to date for spin valves with both inorganic and organic spacer layers. Moreover, a large spin-diffusion length of approximately 81 nm was experimentally obtained for polycrystalline hybrid perovskite films at 10 K under light illumination. Interestingly, because of the photoconductive nature of hybrid perovskites, multiple resistance states were successfully achieved in a single device by tuning the magnetic field and lighting conditions. Furthermore, we investigated spin valves by using thin perovskite single crystals, from which we estimated that the spin-diffusion length reached 950 nm at 10 K. These results indicate that this emerging class of hybrid materials can be used as an effective medium for spin-polarized transport, thus opening a door toward the construction of perovskite-based spintronic devices.

■ RESULTS AND DISCUSSION

Device Structure of the Hybrid Perovskite Spin Valves. Figure 1a shows a schematic diagram of the hybrid perovskite spin valve with a $SrTiO_3$ (STO) substrate/$La_{2/3}Sr_{1/3}MnO_3$ (LSMO)/$MAPbI_3$/Co/Al stacking structure, and the effective device area is approximately 0.2×0.1 mm^2 (see Figure S1). LSMO was chosen as the bottom ferromagnetic (FM) electrode in our devices because of its nearly 100% spin polarization at low temperatures as well as its chemical and environmental stability.[8,37,38] A perovskite layer
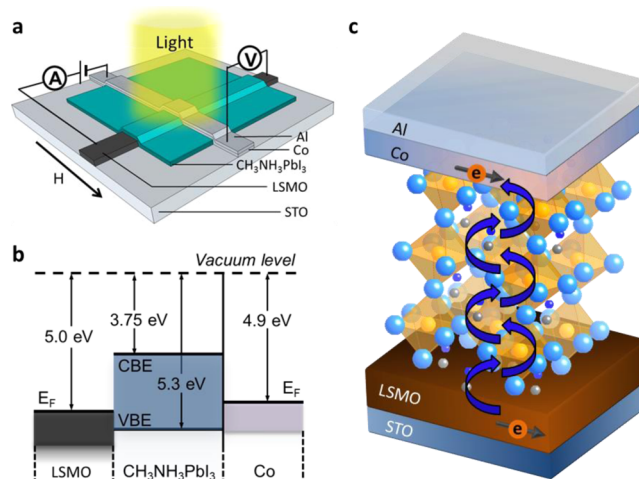

Figure 1. Schematic representation of the perovskite-based spin valve. (a) Device and measurement configuration. A 100 nm epitaxial LSMO layer and a 30 nm Co layer were used as the spin-polarized electrodes. Hybrid perovskite ($MAPbI_3$) layers with different thicknesses (80, 120, 160, and 200 nm) served as the spin-transporting medium in the spin valves. (b) Energy-level diagram for the hybrid perovskite-based device. For simplicity, band bending and possible dipole formation at the interfaces are not illustrated. CBE and VBE stand for conduction band edge and valence band edge, respectively. (c) Schematic representation of the perovskite spin valve, illustrating the spin-polarized carriers being injected from the FM electrodes into the hybrid perovskite layer.

with varied thicknesses ($d = 80−200$ nm) was deposited on the LSMO electrodes through a two-step, vapor-assisted process.[21,23,39] Figure 1b illustrates the Fermi levels (E_F) of two FM electrodes as well as the band edges of the hybrid perovskite, and as we will demonstrate later, Schottky junctions are formed at the electrode/perovskite interfaces. Furthermore, our experimental results support the scenario that spin-polarized carriers are injected from the FM electrodes into the perovskite layer (Figure 1c).

Characterizations of the Magnetic Electrodes and Active Layers. In spintronic devices, retaining high spin polarization in FM electrodes is considered to be a prerequisite for realizing optimal device performance. LSMO films in our experiments were annealed in oxygen under atmospheric pressure at 1050 °C for 6 h prior to the deposition of the perovskite layer, which has been shown to enhance the surface spin polarization of LSMO electrode and thus the MR effect of spin valves.[40] Figure 2a shows the atomic force microscopy (AFM) image of an annealed LSMO film, which has a flat surface with an average terrace width of 150 nm and step height of approximately 0.4 nm, thereby indicating an ordered electrode termination with high crystalline quality. In contrast, the surface of an as-grown LSMO film displayed dense small islands (Figure S2). Furthermore, the X-ray diffraction (XRD) pattern shown in Figure 2b further indicates that the annealed LSMO film was highly crystalline and possessed a high film quality. Figure 2c presents the temperature dependence of magnetization ($M−T$) measured with an in-plane magnetic field of 500 Oe for the annealed LSMO film, which features a sharp FM-to-paramagnetic transition. The Curie temperature (T_C) of the annealed LSMO film reached 368 K, a value comparable to that of the bulk LSMO (ref 41) and much higher than the T_C of the as-grown sample (324 K, Figure S3). Clearly, the annealing process was effective for producing
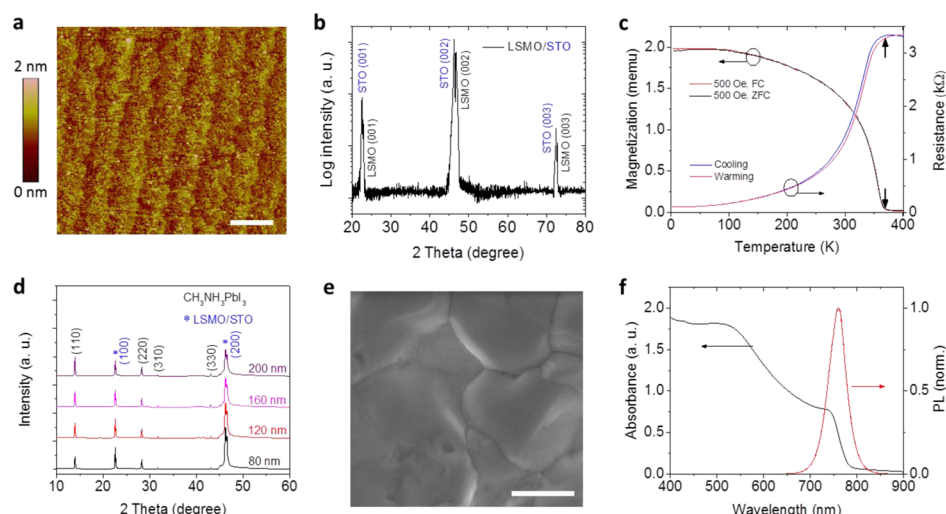
Figure 2. Characterization of the LSMO electrode and the perovskite layers. (a) AFM image of the annealed LSMO film. Scale bar = 1.0 μm. (b) Corresponding XRD pattern. (c) $M–T$ and $R–T$ curves of the LSMO film. Both measurements show a Curie temperature (T_C) of approximately 368 K. For the $M–T$ measurement, the sample was measured under an in-plane magnetic field of 500 Oe. FC: field cooled and ZFC: zero fieled cooled. (d) XRD spectra of the perovskite films with different thicknesses deposited on the LSMO electrodes. (e) Top-view SEM image of the $CH_3NH_3PbI_3$ film with a thickness of 200 nm. Scale bar = 0.5 μm. (f) Absorption and PL spectra of the hybrid perovskite film.
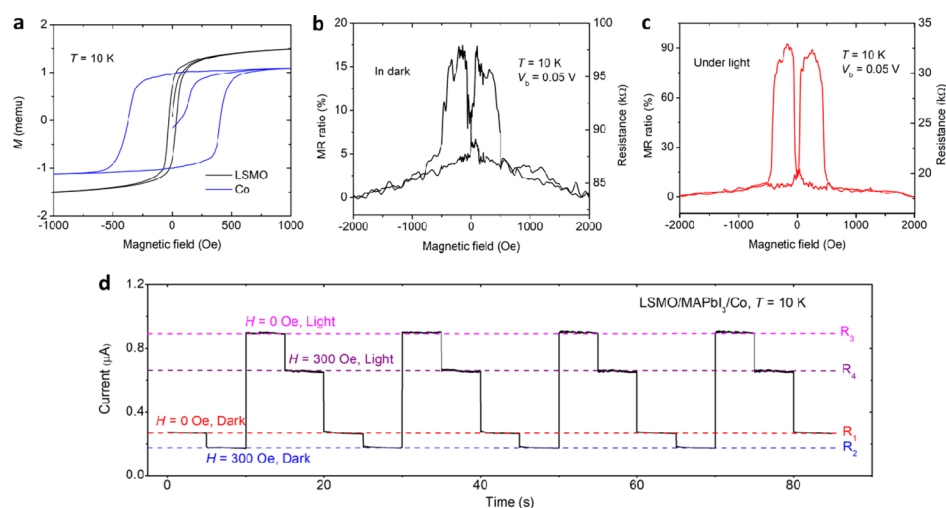
Figure 3. MR of the perovskite spin valve. (a) Magnetic hysteresis curves of the individual LSMO and Co electrodes measured at 10 K. The H_C of LSMO is approximately 50 Oe and that of the Co film is approximately 400 Oe. (b) MR and resistance data of the spin valve composed of an 80 nm perovskite interlayer measured in the dark. (c) MR and resistance data of the device measured under illumination. (d) Realization of four resistance states in a spin valve by controlling the magnetic field and light illumination. In this dynamic measurement, the voltage across the spin valve was set as 0.05 V.

LSMO films with improved oxygen stoichiometry. The high quality of the LSMO film was also supported by the resistance-temperature ($R–T$) data (Figure 2c).

Figure 2d shows the XRD patterns of the MAPbI$_3$ layers deposited onto the LSMO-coated STO substrates with the thicknesses of 80, 120, 160, and 200 nm. The main diffraction peaks at 14.12, 28.44, and 43.23° were assigned to the (110), (220), and (330) planes of the orthorhombic MAPbI$_3$, respectively. As the perovskite thickness increased, these diffraction peaks strengthened, thus indicating better crystallinity in the films. The surface morphology of the MAPbI$_3$ films was evaluated using scanning electron microscopy (SEM), and Figure 2e shows that the perovskite film is smooth and free from any pinholes. The optical absorption and PL spectra of the 200 nm MAPbI$_3$ film are shown in Figure 2f. The strong and broad absorption in the

UV–vis range, particularly from 400 to 780 nm, reveals that the perovskite layer is a good light absorber.[13–15,21] A strong near-infrared PL peak at approximately 770 nm was observed, which is consistent with the band gap of MAPbI$_3$.[13–15]

Hysteresis Curves and Spin Transport Properties. The operation of spin valves requires that the two FM electrodes switch at different external magnetic fields. Figure 3a shows that the coercivities (H_C) of LSMO and Co electrodes at 10 K are 50 and 400 Oe, respectively. These different values in the H_C enable antiparallel and parallel magnetization alignments, a precondition for realizing discreet resistance states in spin valves. The related magnetization hysteresis loop of a spin-valve device measured at 10 K is shown in Figure S4, which indicates a two-step switching of the total magnetization. This is a characteristic behavior of a spin-valve device where the high- and low-resistance states come from the configurations of
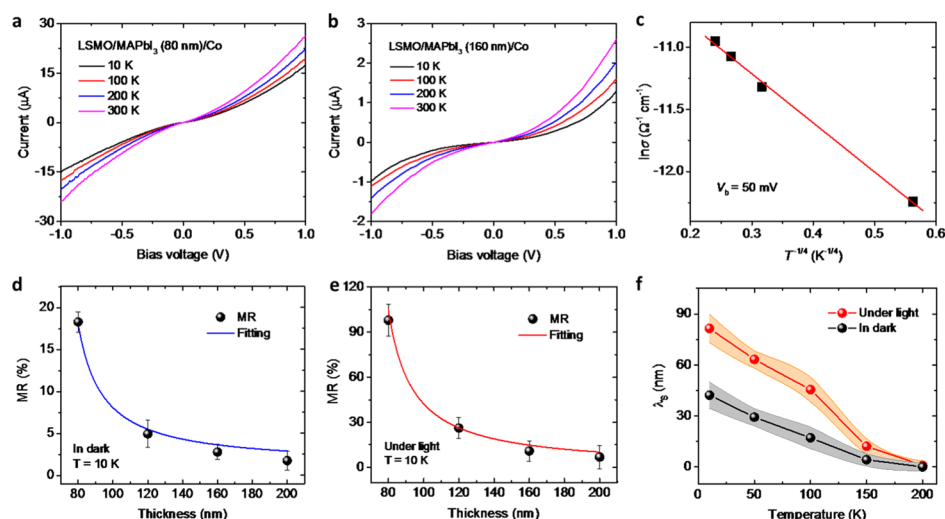
Figure 4. Spin transport properties of perovskite films. (a) Nonlinear $I-V$ curves for the spin valve with an 80 nm perovskite layer measured in the dark at different temperatures. (b) $I-V$ curves at different temperatures for the spin valve with a hybrid perovskite interlayer of 160 nm. (c) Logarithmic conductance as a function of temperature $T^{-1/4}$, revealing the hopping nature of carrier transport. The line in (c) is linear fitting. (d) Thickness-dependent MR measured at 10 K in the dark. A spin-diffusion length of approximately 42.3 nm was derived from fitting the data to the modified Julliere formula. (e) Under light illumination, the spin-diffusion length reached 81.4 nm at 10 K. (f) Temperature-dependent spin-diffusion length measured from 20 devices. The shaded regions represent the error bars. The spin-diffusion length under illumination was much higher than that under dark conditions, and it decreased with increasing temperature.

antiparallel and parallel alignments of the magnetization of the FM layers, respectively. Figure 3b,c show the MR loops of an 80 nm perovskite device measured at 10 K, in the dark and under illumination, respectively. As expected, the MR of the spin valve switched at the coercive fields of LSMO and Co, a result consistent with the magnetization data in Figure 3a. The MR ratio was calculated using the expression $\Delta R/R_P = (R_{AP} - R_P)/R_P \times 100\%$, where R_{AP} and R_P stand for the resistances in the antiparallel and parallel states, respectively, and R_P was obtained at a magnetic field of 2000 Oe. The MR ratio was 18.2% for the 80 nm perovskite device (Figure 3b), and it monotonously decreased with an increasing film thickness (Figure S5a). These MR data were collected under an applied bias of just 50 mV, and such a low bias is crucial for low-power device operations. When measured at 100 K in the dark, the MR ratio for the 80 nm perovskite device decreased to approximately 7.3% (Figure S6a). Moreover, the MR ratio steeply decayed with increasing temperature, in agreement with the results from previous reports on spin valves.[6−10,42−48]

The photoresponsive nature of perovskites presents a new dimension for modulating the spin transport in such hybrid spintronic devices. After characterizing the basic properties of our devices, we further explored the effect of light illumination on spin transport in the hybrid perovskite layers. As shown in Figures 3c and S5b, when the devices were measured under illumination, the MR significantly increased. For the 80 nm perovskite device, the MR values under different power densities are shown in Figure S7. The MR ratio reached 97.4% at 10 K and under an illumination of 10 mW cm^{-2}, a value on par with the highest values ever reported for organic and inorganic spin valves (Table S2).[2−10,42−48] Furthermore, the MR of the hybrid spin valve decreased with increasing temperature (Figures S5 and S6), similar to the case performed in the dark.

To exclude the possibility that the observed MR originated from the anisotropic MR effects of the FM electrodes, the magnetotransport properties of the LSMO strips were

evaluated at different temperatures. The MR ratio of the LSMO electrode at a high magnetic field of ±10 000 Oe was below 0.2% (Figure S8), a value 500 times lower than that measured from our perovskite devices. This result confirmed that the observed MR of the spin valves was not caused by the anisotropic MR effect of the FM electrodes but instead should be attributed to the spin-dependent transport across the hybrid perovskite layer.

As shown in Figures 3b,c and S5, the magnitude of MR steeply decreased as the thickness of the perovskite interlayer increased. However, a reasonably high MR ratio of 0.8% was still achieved at 10 K in the 200 nm perovskite spin valve, and more remarkably, the same device showed a MR of 6.4% at 10 K under illumination. To the best of our knowledge, the obtained MR value is among the highest values ever reported for spin valves with such a thick active layer, thus indicating the capability of hybrid perovskites to serve as a good medium for spin transport. Furthermore, the fact that the overall resistance in the dark (Figure 3b) is much higher than that under illumination (Figure 3c) in the same device implies that the current flowing through the junction is photosensitive, favoring the efficient injection and transportation of spin-polarized carriers. In addition to being a solid evidence for spin transport across the perovskite layer, the light sensitivity adds functionality to the device.

All devices exhibited a steep decrease in their MR ratios with increasing temperature, and negligible MR values were observed at room temperature (RT). This temperature dependence on the MR is consistent with previously reported results on organic spin valves with LSMO electrodes[6−8,10,44,47,49] and can be attributed to the weakened surface spin polarization of LSMO at high temperatures and the surface antiferromagnetism.[50] Additionally, the possible relaxation of spin polarization within the perovskite interlayer and at the FM/perovskite interface may also play a role.

Importantly, the light sensitivity of the perovskite spacer layer adds a new optical tuning parameter to the operation of
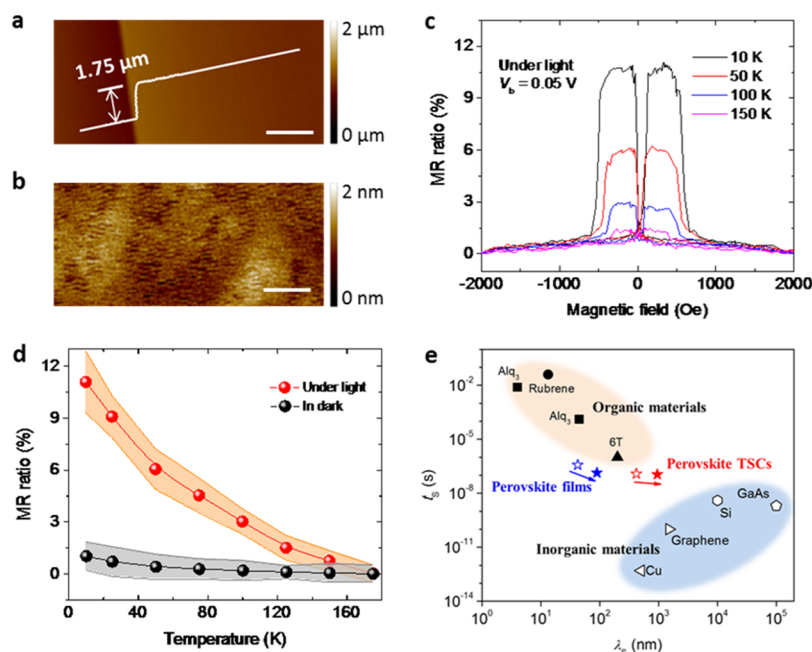
Figure 5. Spin valves based on thin perovskite single crystals. (a) AFM image taken near the edge of a TSC grown on the LSMO film. Scale bar = 2.0 μm. (b) AFM image of the TSC surface, showing a low RMS roughness of 0.17 nm. Scale bar = 200 nm. (c) MR curves of spin valves based on TSCs measured at different temperatures under illumination. (d) Temperature-dependent MR measured from 12 single-crystal spin-valve devices. The shaded regions in this figure represent the error bars. (e) Chart of the spin relaxation time (t_S) vs the spin-diffusion length (λ_S) for the hybrid perovskites compared to several typical organic and inorganic materials. Empty and filled stars represent the spin transport parameters measured at 10 K in the dark and under illumination, respectively.

our spin valves, in addition to the conventional magnetic field. Figure 3d shows the consecutive switching between the four current states of a device based on an 80 nm active perovskite layer at 10 K and a low bias of 0.05 V. Clearly, more current states of such heterojunctions can be created by concurrently tuning the light irradiation and magnetic field, thereby indicating the possibility of creating multi-bit storage devices using perovskite spin valves, which has also been reported in the spin valve based on the photosensitive semiconducting materials.[34−36,51]

Current−Voltage (*I−V*) Characteristics of the Hybrid Perovskite Spin Valves. To gain deeper insights into the mechanism of spin-polarized transport in the perovskite spin valves, current−voltage (*I−V*) characteristics were measured at different temperatures. Figure 4a,b show that the *I−V* curves measured on perovskite spin valves with two different spacer thicknesses are clearly nonlinear, a result consistent with the high-quality perovskite layers being free of pinholes; otherwise, any direct contact between the FM electrodes would lead to Ohmic transport. Moreover, the temperature dependence of the conductivity ($\sigma−T$) in the perovskite spin valve obeyed the relationship $\sigma = \sigma_0 \exp(−T_0/T)^{1/4}$ in the temperature range of 10−300 K (Figure 4c), a characteristic of variable range hopping transport.[52] This analysis indicates that after the spin-polarized charge carriers are injected from the FM (LSMO and Co) electrodes, they transmit through the perovskite interlayer by hopping. In fact, the hopping of charge carriers and the associated spin precession are the essential elements for spin diffusion in disordered OSCs.[53,54] Furthermore, by using the space charge-limited current (SCLC) method, the carrier mobility in polycrystalline perovskite films, measured at RT, in the dark and upon illumination was estimated as 0.044 and 0.53 cm^2 V^{-1} s^{-1}, respectively (Figures S9 and S10), which is close to the value reported for OSCs like C$_{60}$[55] and much

lower than those of high-quality inorganic semiconductors (e.g., over 1000 cm^2 V^{-1} s^{-1} for crystalline silicon).[56] This comparison indicates that although hybrid perovskites do not feature π-conjugated molecular interactions like OSCs, defect trapping and hopping transport contribute to the spin-diffusion characteristics in this new class of spintronic medium.

As shown in Figure S11a, the *I−V* curves of our perovskite devices were dramatically modulated by light irradiation and the photocurrent is more than three times larger than the dark current. Since the FM LSMO and Co electrodes are weak in light absorption, this result suggests that the junction transport is dominated by the photoactive perovskite interlayer. At $V_b =$ −1 V, the conductance under illumination was almost threefold higher than that in the dark. The light-modulated transport can be elucidated by considering the band diagram shown in Figure 1b. The LSMO/perovskite/Co heterojunction can be treated as a back-to-back diode, in which the Schottky barriers can also contribute to the device resistance. Correspondingly, the junction conduction can be described by the Schottky thermionic emission model[57,58]

$$I(V_b) = A^*AT^2 \exp\left[\left(-\frac{e\phi_B}{k_BT}\right)\right]\left[\exp\left(\frac{eV_b}{k_BT}\right) - 1\right] \quad (1)$$

where A^* is the standard Richardson constant, A is the junction area, and ϕ_B is the Schottky barrier height. By fitting the *I−V* data to eq 1, ϕ_B was estimated to be 0.21 and 0.13 eV in the dark and under illumination, respectively (see Figure S11b,c). Therefore, a reduction of the Schottky barriers underlies the light-induced modulation of the junction conductivity, which facilitates the spin-polarized injection at the FM electrode/perovskite interfaces and improves the device performance.

To elucidate the origin of the high MR in the perovskite spin valves, we applied the modified Julliere formula to characterize the MR characteristics.[6,7,59] As a result of the decay of the spin polarization of injected carriers in the perovskite interlayer, the MR ratio should have the following dependence on the perovskite active layer thickness, d

$$\text{MR} = \frac{2p_1 p_2 \ e^{-(d-d_0)/\lambda_S}}{1 - p_1 p_2 \ e^{-(d-d_0)/\lambda_S}} \tag{2}$$

where $p_1 p_2$ denotes the product of the spin polarizations of the FM electrodes and d_0 is the thickness of the "ill-defined" layer formed during device fabrication.[8] As shown in Figure 4d, a good fitting was observed for the MR data measured at 10 K in the dark, and the spin-diffusion length λ_S was extracted as 42 nm. Furthermore, we fitted the MR data measured under illumination to the Julliere formula and obtained $\lambda_S = 81$ nm and $d_0 = 47$ nm at 10 K (Figure 4e). Table S1 summarizes the $p_1 p_2$ values, which were obtained by fitting the MR-thickness data at different temperatures using the Julliere formula.

In order to investigate interface diffusion in the perovskite layer during Co deposition, cross-sectional transmission electron microscopy and elementary mapping by energy dispersive X-ray spectroscopy were performed. Figure S12a shows the microscopy images of all layers in the perovskite spin valve. It can be found that the interface between the perovskite layer and the Co electrode is not very sharp, which is confirmed by the elemental mapping result (Figure S12b−f). These data directly demonstrate that there is appreciable diffusion of Co into the hybrid perovskite layer, leading to the formation of an "ill-defined" layer in the perovskite spin valve.

Figure 4f shows the temperature dependence of the spin-diffusion length λ_S measured from 20 devices both in the dark and under illumination, which exhibits a steep decrease with increasing temperature, and λ_S becomes negligible above 200 K, in agreement with the previously reported results for organic spin valves.[6–10] More importantly, the values of λ_S measured under illumination were markedly enhanced compared with those measured in the dark, a result that can be attributed to the reduction of the Schottky barrier and the improved mobility in the light-illuminated perovskites.[21] According to the relationship between λ_S and μ, $\lambda_S = \sqrt{(k_B T/e)\mu t_S}$, the higher μ achieved under illumination should improve both MR and λ_S of the hybrid perovskite spin valves.

Spin Transport of the Perovskite Single-Crystal Devices. Because single crystals are free of grain boundaries and structural defects, better charge and spin transport properties are expected if the perovskite single crystals are thin enough that spin-polarized carriers can transmit through. We fabricated spin valves using thin single crystals (TSCs) of MAPbBr$_3$ and explored the spin transport in TSCs. The TSCs were prepared using a geometry-confined method in which the growth occurred between two substrates separated by two thin spacers (ref 60, see Figure S13). Figure 5a shows the AFM image taken near the edge of the TSC, indicating a thickness of approximately 1.75 μm. As shown in the AFM image in Figure 5b, the TSC had a smooth surface with an RMS roughness of only 0.2 nm, thereby indicating the potential of achieving a much smaller "ill-defined" layer in the TSC-based spin valves. SEM characterization further confirmed the highly homogeneous and boundary-free surface of the TSC (Figure S14), a

characteristic highly beneficial for achieving a high-quality Co/perovskite interface. The XRD measurement indicated the high crystallinity of the TSC (Figure S15a). The optical absorption and PL spectra of the TSC shown in Figure S14b reveal that the TSC is a good light absorber with sharp band-edge optical transitions. The carrier mobilities of our TSCs at RT were estimated to be 48 cm^2 V^{-1} s^{-1} by using the SCLC method (Figures S16 and S17). Despite the low thickness, the as-grown TSCs exhibited good transport properties with low trap densities comparable to those of the highest quality MAPbBr$_3$ samples reported to date.[27]

Figure 5c shows the typical MR response of a spin valve based on TSCs measured under illumination at various temperatures (10, 50, 100, and 150 K). The steps of the MR curves were consistent with the H_C for the LSMO and Co electrodes. Notably, a reasonably high MR ratio of 11.2% was achieved at 10 K and under illumination. As shown in Figure S18, when the device was measured in the dark, the MR significantly decreased, and its ratio was approximately 1.1% at 10 K, a value just one-tenth that measured under illumination. These MR values were notable, given that they were collected in spin valves with micrometer-thick active perovskite layers. Figure 5d summarizes the MR values of the 12 TSC-based spin valves measured in the dark and under illumination at different temperatures. The MR ratio steeply decayed with increasing temperature, a result consistent with findings from previous reports.[6–10]

Furthermore, the λ_S value within the TSC was estimated on the basis of the MR data. Considering the low surface roughness of the TSC (Figure 5b), we set $d_0 = 0$, and then eq 2 was simplified as follows

$$\text{MR} = \frac{2p_1 p_2 \ e^{-d/\lambda_S}}{1 - p_1 p_2 \ e^{-d/\lambda_S}} \approx 2p_1 p_2 \ e^{-d/\lambda_S} \tag{3}$$

Because of the smooth LSMO/TSC and TSC/Co interfaces, high spin polarizations of the FM electrodes are expected. Using $p_1 p_2 = 35\%$ at 10 K (refs 8, 61) and $d = 1750$ nm, λ_S was extracted as 950 nm under light illumination. Similar to the case of polycrystalline perovskite films, light illumination was found to effectively enhance λ_S in the TSC.

The spin relaxation time, t_S, is related to the spin-diffusion length λ_S through the following equation: $\lambda_S = \sqrt{(k_B T/e)\mu t_S}$.[6,7,62] As shown in Figure S16, the measured carrier mobility of high-quality perovskite single crystals is approximately 94 cm^2 V^{-1} s^{-1} at low temperatures. Thus, the t_S in the TSCs was estimated to be 110 ns under light illumination, which is comparable to the carrier lifetime measured on similar perovskite single crystals.[27,28]

During the development of spintronics, both organic and inorganic materials have been explored as the medium for spin transport. Figure 5e summarizes the t_S versus λ_S data for some typical materials investigated in the context of spin valves (Table S1).[6,7] The notable feature emerging from the chart is that organic materials occupy the top-left region; that is, they are characterized by long t_S and short λ_S values. In organic materials, spins can survive for certain periods of time but do not travel far. This behavior may be easily understood because the mobility of organic materials is usually low. Although inorganic materials possess much longer λ_S as a result of their high mobility, they have the drawback of short t_S and fast spin relaxation. Although hybrid perovskites possess well-defined

band structures like inorganic semiconductors, their hopping transport in spin valves is similar to organic materials. Interestingly, as an emerging class of spintronic materials, the hybrid perovskites exhibited strongly enhanced λ_S compared with those of organic materials, and the spin-polarized carriers were able to diffuse on the order of hundreds of nanometers in the hybrid perovskite layers without losing their spin polarization. It is also a general observation that light illumination is effective to enhance the spin-diffusion length in hybrid perovskite for both polycrystalline films and single crystals. Furthermore, the hybrid perovskites possessed relatively large t_S, indicating that the spins relax much slower than most inorganic materials. Clearly, as shown in Figure 5e, hybrid perovskites have a unique position among the spin transport mediums, bridging the organic and inorganic counterparts.

Discussion on the Spin Relaxation Mechanism in Hybrid Perovskites. It is generally believed that the presence of heavy atoms would enhance SOC and HFI, thereby accelerating the spin relaxation. However, in the hybrid perovskite spin valves, although heavy atoms (Pb, I) exist in the perovskite layer, we obtained a large MR effect. Recent theoretical calculations have revealed that the conduction band edge of hybrid perovskites is mainly composed of the p-orbital of Pb, whereas the valence band edge has a strong Pb-s and I-p antibonding character.[63] Because the perovskite films are p-type, s-electrons of Pb dominate the spin transport. Generally, the intrinsic SOC of the s-orbital is approximately zero, although high-order interactions due to various reasons may lead to small contributions. As a result, SOC at the valence band edge is weak,[64] and thus, we can exclude SOC as the dominant mechanism for the spin relaxation in hybrid perovskite. However, we should note that if n-type perovskite films are prepared by adjusting the synthesis conditions, the SOC may be much enhanced.

We can also conclude that the Elliott–Yafet mechanism appears to be less likely as the dominant mechanism for the spin relaxation because this mechanism was developed to take account of the SOC effect.[65] In the D'yakonov–Perel' mechanism,[66] the prerequisite for an effective magnetic field is the breaking of the inversion symmetry, which is absent in the perovskite layer. Furthermore, the spin relaxation time of the perovskite single crystal is similar to that of a polycrystalline film, although the mobility of the former increases by a factor of ~50 compared to the latter; in other words, the spin relaxation time is not sensitively dependent on disorder, making the conventional DP and EY mechanisms unlikely.[67]

Finally, in the HFI mechanism,[53] λ_S can be generally written as $\lambda_S \propto \sqrt{Dt_S} \propto \mu$, which is consistent with our observations. HFI is a major source for spin scattering in OSCs as a result of hydrogen atoms. However, in hybrid perovskites, charge transport occurs dominantly through the network of Pb-halide octahedra, and the conduction band edge of hybrid perovskites is mainly composed of the Pb p-orbital. As a result, HFI may not work as the dominant spin relaxation mechanism in such hybrid materials.

■ CONCLUSIONS

In summary, we demonstrated that hybrid perovskites can be used as a new spin-diffusion medium in spintronic devices, and our results revealed that the photoactive nature of the perovskites allows both applied magnetic fields and light

illumination as operational parameters. A high MR of up to 97% was achieved at low temperatures. Furthermore, a spin-diffusion length of 81 nm was observed in the polycrystalline perovskite films under illumination, and it could be enhanced to approximately 1 μm through the use of thin perovskite single crystals as the active layers in the spin valves. It seems that the common mechanisms, including SOC and HFI, may not cause significant spin relaxation in such hybrid materials. Interestingly, owing to the multifunctional character of the hybrid perovskite films, MR and photoresponse were simultaneously observed under low operation biases, realizing multiple resistance states in a single device. Our findings indicate the potential application of hybrid perovskites in flexible magnetic field sensors, solution-processed nonvolatile memories, and other photoactive spintronic devices.

■ EXPERIMENTAL DETAILS

Sample Fabrication. LSMO films with a thickness of 100 nm were deposited on STO(100) substrates using pulsed laser deposition through a shadow mask, thus forming 0.1 mm wide stripes as the bottom electrodes. These LSMO electrodes were annealed at 1050 °C for 6 h under flowing pure oxygen to achieve optimal magnetic properties. After plasma cleaning, the LSMO films were introduced into an evaporation chamber, and a lead(II) iodide layer (PbI$_2$, Sigma-Aldrich, 98%) was thermally evaporated onto the films. On a hot plate, methylammonium iodide powders (CH$_3$NH$_3$I, Sigma-Aldrich) were spread around the PbI$_2$-coated substrates, and a Petri dish was placed over the samples. After heating at 150 °C for 8 h, the as-prepared films were washed with isopropanol and dried at 65 °C for 5 min. Finally, a 30 nm Co film (capped with a 15 nm Al) was thermally evaporated as the top FM electrode by using a shadow mask. During the deposition of the Co layer, a carefully tailored low-power evaporation process was applied to prevent damage to the perovskite layer from heat irradiation during the Co deposition. All fabrication steps involving the hybrid perovskite layers and the top electrodes were performed inside a glovebox or inside a glovebox-integrated vacuum evaporator.

For the thin perovskite single-crystal fabrication, 2.0 μm poly-ethylene terephthalate (PET) thin strips were first attached on top of the substrates and then covered by a glass slide. After annealing on a hot plate at 270 °C for 5 min, the PET melted and adhered the substrate and the glass covers together. Perovskite precursor solutions were introduced between the two slides, and TSCs were then formed between the two slides under heating. The distance between the two slides was found to effectively limit the thickness of the resulting TSCs.

Characterizations. XRD was performed on a Bruker D8-Advance diffractometer using Cu Kα radiation (λ = 1.5406 Å). The morphology of the LSMO electrodes and perovskite films was measured using an AFM (Bruker, Dimension ICON). A field-emission SEM (FEI Nova Nano 630) was used to acquire the SEM images. The absorption and steady-state PL were recorded using a Cary 6000i spectrophotometer with an Edinburgh Instrument spectrofluorometer. The magnetic properties of the FM electrodes were measured with a Quantum Design superconducting quantum interference device magnetometer. The MR measurements of the spin valves were performed under an in-plane magnetic field using the standard four-probe method in a Quantum Design physical property measurement system equipped with a laser beam (532 nm) with varied light power densities. For the TSC-based spin valves, the MR measurements from RT to 10 K were performed in an EMPX-HF probe station equipped with a UV LED. The current–voltage ($I–V$) measurements were conducted using a Signotone micromanipulator S-1160 probe station equipped with a laser beam and Keithley 4200 SCS.

■ ASSOCIATED CONTENT

Ⓢ Supporting Information

The Supporting Information is available free of charge at https://pubs.acs.org/doi/10.1021/acsami.9b18562.

A hybrid-perovskite spin valve, AFM image of the as-grown LSMO film, $M-T$ curves of the as-grown and annealed LSMO films, MR curves of the spin valves with different perovskite layer thicknesses measured at different temperatures, MR curves of the device under different power densities, anisotropic MR ratios of the LSMO film, $I-V$ characteristics of devices under different conditions, Schottky barrier height analysis, microstructure of a hybrid perovskite-based spin valve, schematic for geometry-confined method, SEM image, XRD pattern, absorption and PL spectra of the TSC, $I-V$ characteristics of the perovskite TSC under different conditions, MR curves of the perovskite single crystal spin valves, p_1p_2 values at different temperatures, and the device performance of some typical spin valves (PDF)

■ AUTHOR INFORMATION

Corresponding Author
*E-mail: tom.wu@unsw.edu.au.

ORCID Ⓘ
Feng Li: 0000-0003-4448-074X
Weili Yu: 0000-0001-5075-9638
Tom Wu: 0000-0003-0845-4827

Present Address
#Key Laboratory of Materials Physics, Institute of Solid State Physics, Chinese Academy of Sciences (CAS), Hefei 230031, People's Republic of China.

Notes
The authors declare no competing financial interest.

■ ACKNOWLEDGMENTS

■ REFERENCES

(1) Žutić, I.; Fabian, J.; Das Sarma, S. Spintronics: fundamentals and applications. *Rev. Mod. Phys.* **2004**, *76*, 323−410.
(2) Fert, A. Nobel Lecture: Origin, development, and future of spintronics. *Rev. Mod. Phys.* **2008**, *80*, 1517−1530.
(3) Wolf, S. A.; et al. Spintronics: A spin-based electronics vision for the future. *Science* **2001**, *294*, 1488−1495.
(4) Appelbaum, I.; Huang, B.; Monsma, D. J. Electronic measurement and control of spin transport in silicon. *Nature* **2007**, *447*, 295−298.
(5) Jansen, R. Silicon spintronics. *Nat. Mater.* **2012**, *11*, 400−408.
(6) Szulczewski, G.; Sanvito, S.; Coey, M. A spin of their own. *Nat. Mater.* **2009**, *8*, 693−695.
(7) Sanvito, S. Molecular spintronics. *Chem. Soc. Rev.* **2011**, *40*, 3336−3355.
(8) Xiong, Z. H.; Wu, D.; Valy Vardeny, Z.; Shi, J. Giant magnetoresistance in organic spin-valves. *Nature* **2004**, *427*, 821−824.
(9) Dediu, V. A.; Hueso, L. E.; Bergenti, I.; Taliani, C. Spin routes in organic semiconductors. *Nat. Mater.* **2009**, *8*, 707−716.
(10) Devkota, J.; Geng, R.; Subedi, R. C.; Nguyen, T. D. Organic Spin Valves: A Review. *Adv. Funct. Mater.* **2016**, *26*, 3881−3898.
(11) Burschka, J.; et al. Sequential deposition as a route to high-performance perovskite-sensitized solar cells. *Nature* **2013**, *499*, 316−319.
(12) Jeon, N. J.; et al. Solvent engineering for high-performance inorganic−organic hybrid perovskite solar cells. *Nat. Mater.* **2014**, *13*, 897−903.
(13) Gao, P.; Grätzel, M.; Nazeeruddin, M. K. Organohalide lead perovskites for photovoltaic applications. *Energy Environ. Sci.* **2014**, *7*, 2448−2463.
(14) Stranks, S. D.; Snaith, H. J. Metal-halide perovskites for photovoltaic and light-emitting devices. *Nat. Nanotechnol.* **2015**, *10*, 391−402.
(15) Tan, Z.-K.; et al. Bright light-emitting diodes based on organometal halide perovskite. *Nat. Nanotechnol.* **2014**, *9*, 687−692.
(16) Chin, X. Y.; Cortecchia, D.; Yin, J.; Bruno, A.; Soci, C. Lead iodide perovskite light-emitting field-effect transistor. *Nat. Commun.* **2015**, *6*, 7383.
(17) Zhu, H.; et al. Lead halide perovskite nanowire lasers with low lasing thresholds and high quality factors. *Nat. Mater.* **2015**, *14*, 636−642.
(18) Dou, L.; et al. Solution-processed hybrid perovskite photodetectors with high detectivity. *Nat. Commun.* **2014**, *5*, 5404.
(19) Dong, R.; et al. High-gain and low-driving-voltage photodetectors based on organolead triiodide perovskites. *Adv. Mater.* **2015**, *27*, 1912−1918.
(20) Alwadai, N.; et al. High-performance ultraviolet-to-infrared broadband perovskite photodetectors achieved via inter-/intraband transitions. *ACS Appl. Mater. Interfaces* **2017**, *9*, 37832−37838.
(21) Li, F.; Ma, C.; Wang, H.; Hu, W.; Yu, W.; Sheikh, A. D.; Wu, T. Ambipolar solution-processed hybrid perovskite phototransistors. *Nat. Commun.* **2015**, *6*, 8238.
(22) Li, F.; et al. Ultrahigh carrier mobility achieved in photo-responsive hybrid perovskite films via coupling with single-walled carbon nanotubes. *Adv. Mater.* **2017**, *29*, 1602432.
(23) Guan, X.; et al. P-type SnO thin film phototransistor with perovskite-mediated photogating. *Adv. Electron. Mater.* **2019**, *5*, 1800538.
(24) Ha, S.-T.; Shen, C.; Zhang, J.; Xiong, Q. Laser cooling of organic−inorganic lead halide perovskites. *Nat. Photonics* **2016**, *10*, 115−121.
(25) Xing, G.; et al. Long-range balanced electron- and hole-transport lengths in organic-inorganic $CH_3NH_3PbI_3$. *Science* **2013**, *342*, 344−347.
(26) Stranks, S. D.; et al. Electron-hole diffusion lengths exceeding 1 micrometer in an organometal trihalide perovskite absorber. *Science* **2013**, *342*, 341−344.
(27) Shi, D.; et al. Low trap-state density and long carrier diffusion in organolead trihalide perovskite single crystals. *Science* **2015**, *347*, 519−522.
(28) Dong, Q.; et al. Electron-hole diffusion lengths > 175 mm in solution-grown $CH_3NH_3PbI_3$ single crystals. *Science* **2015**, *347*, 967−970.
(29) Zhang, C.; et al. Magnetic field effects in hybrid perovskite devices. *Nat. Phys.* **2015**, *11*, 427−434.
(30) Hsiao, Y.-C.; et al. Magneto-optical studies on spin-dependent charge recombination and dissociation in perovskite solar cells. *Adv. Mater.* **2015**, *27*, 2899−2906.
(31) Wang, J.; et al. Spin-optoelectronic devices based on hybrid organic-inorganic trihalide perovskites. *Nat. Commun.* **2019**, *10*, 129.
(32) Wang, J.; et al. Tunable spin characteristic properties in spin valve devices based on hybrid organic−inorganic perovskites. *Adv. Mater.* **2019**, *31*, 1904059.
(33) Yang, Y.; et al. Unexpected Outstanding Room Temperature Spin Transport Verified in Organic−Inorganic Hybrid Perovskite Film. *J. Phys. Chem. Lett.* **2019**, *10*, 4422−4428.
(34) Sun, X.; et al. A molecular spin-photovoltaic device. *Science* **2017**, *357*, 677−680.
(35) Yin, L.; Wang, X.; Mi, W. Ferromagnetic, ferroelectric, and optical modulated multiple resistance states in multiferroic tunnel junctions. *ACS Appl. Mater. Interfaces* **2019**, *11*, 1057−1064.
(36) Han, X.; Mi, W.; Wang, X. Large magnetoresistance and spin-polarized photocurrent in $La_{2/3}Sr_{1/3}MnO_3(Co)$/quaterthiophene/

$La_{2/3}Sr_{1/3}MnO_3$ organic magnetic tunnel junctions. *J. Mater. Chem. C* **2019**, *7*, 4079−4088.

(37) Bowen, M.; et al. Nearly total spin polarization in $La_{2/3}Sr_{1/3}MnO_3$ from tunneling experiments. *Appl. Phys. Lett.* **2003**, *82*, 233−235.

(38) Ding, J.; et al. Manganite/cuprate superlattice as artificial reentrant spin glass. *Adv. Mater. Interfaces* **2016**, *3*, 1500676.

(39) Chen, Q.; et al. Planar heterojunction perovskite solar cells via vapor-assisted solution process. *J. Am. Chem. Soc.* **2014**, *136*, 622−625.

(40) Chen, B. B.; et al. Giant magnetoresistance enhancement at room-temperature in organic spin valves based on $La_{0.67}Sr_{0.33}MnO_3$ electrodes. *Appl. Phys. Lett.* **2013**, *103*, 072402.

(41) Urushibara, A.; Moritomo, Y.; Arima, T.; Asamitsu, A.; Kido, G.; Tokura, Y. Insulator-metal transition and giant magnetoresistance in $La_{1-x}Sr_xMnO_3$. *Phys. Rev. B: Condens. Matter Mater. Phys.* **1995**, *51*, 14103−14109.

(42) Pailloux, F.; et al. Nanoscale analysis of a $SrTiO_3$/$La_{2/3}Sr_{1/3}MnO_3$ interface. *Phys. Rev. B: Condens. Matter Mater. Phys.* **2002**, *66*, 014417.

(43) Dediu, V.; et al. Room-temperature spintronic effects in Alq_3-based hybrid devices. *Phys. Rev. B: Condens. Matter Mater. Phys.* **2008**, *78*, 115203.

(44) Barraud, C.; et al. Unravelling the role of the interface for spin injection into organic semiconductors. *Nat. Phys.* **2010**, *6*, 615−620.

(45) Zhang, X.; et al. Observation of a large spin-dependent transport length in organic spin valves at room temperature. *Nat. Commun.* **2013**, *4*, 1392.

(46) Sun, X.; et al. Room-temperature air-stable spin transport in bathocuproine-based spin valves. *Nat. Commun.* **2013**, *4*, 2794.

(47) Li, F.; et al. Excellent spin transport in spin valves based on the conjugated polymer with high carrier mobility. *Sci. Rep.* **2015**, *5*, 9355.

(48) Li, K.-S.; et al. Organic spin valves with inelastic tunneling characteristics. *Phys. Rev. B: Condens. Matter Mater. Phys.* **2011**, *83*, 172404.

(49) Steil, S.; et al. Spin-dependent trapping of electrons at spinterfaces. *Nat. Phys.* **2013**, *9*, 242−247.

(50) Cossu, F.; et al. Surface antiferromagnetism and incipient metal-insulator transition in strained manganite films. *Phys. Rev. B: Condens. Matter Mater. Phys.* **2013**, *87*, 214420.

(51) Sun, X.; et al. Active Morphology control for concomitant long distance spin transport and photoresponse in a single organic device. *Adv. Mater.* **2016**, *28*, 2609−2615.

(52) Mott, N. F. Conduction in glasses containing transition metal ions. *J. Non-Cryst. Solids* **1968**, *1*, 1−17.

(53) Bobbert, P. A.; Wagemans, W.; van Oost, F. W. A.; Koopmans, B.; Wohlgenannt, M. Theory for spin diffusion in disordered organic semiconductors. *Phys. Rev. Lett.* **2009**, *102*, 156604.

(54) Geng, R.; et al. Engineering of Spin Injection and Spin Transport in Organic Spin Valves Using π-Conjugated Polymer Brushes. *Adv. Funct. Mater.* **2016**, *26*, 3999−4006.

(55) Itaka, K.; et al. High-mobility C_{60} field-effect transistors fabricated on molecular- wetting controlled substrates. *Adv. Mater.* **2006**, *18*, 1713−1716.

(56) Ludwig, G. W.; Watters, R. L. Drift and Conductivity Mobility in Silicon. *Phys. Rev.* **1956**, *101*, 1699.

(57) Sze, S. M.; Ng, K. K. *Physics of Semiconductor Devices*, 3rd ed.; Wiley, 2007.

(58) Guan, X.; et al. Light-responsive ion-redistribution-induced resistive switching in hybrid perovskite schottky junctions. *Adv. Funct. Mater.* **2018**, *28*, 1704665.

(59) Julliere, M. Tunneling between ferromagnetic films. *Phys. Lett. A* **1975**, *54*, 225−226.

(60) Yu, W.; et al. Single crystal hybrid perovskite field-effect transistors. *Nat. Commun.* **2018**, *9*, 5354.

(61) Tedrow, P. M.; Meservey, R. Spin Polarization of Electrons Tunneling from Films of Fe, Co, Ni, and Gd. *Phys. Rev. B: Solid State* **1973**, *7*, 318−326.

(62) Nguyen, T. D.; et al. Isotope effect in spin response of π-conjugated polymer films and devices. *Nat. Mater.* **2010**, *9*, 345−352.

(63) Yin, W.-J.; Yang, J.-H.; Kang, J.; Yan, Y.; Wei, S.-H. Halide perovskite materials for solar cells: a theoretical review. *J. Mater. Chem. A* **2015**, *3*, 8926−8942.

(64) Kim, M.; Im, J.; Freeman, A. J.; Ihm, J.; Jin, H. Switchable S = 1/2 and J = 1/2 Rashba bands in ferroelectric halide perovskites. *Proc. Natl. Acad. Sci. U.S.A.* **2014**, *111*, 6900−6904.

(65) Elliott, R. J. Theory of the effect of spin-orbit coupling on magnetic resonance in some semiconductors. *Phys. Rev.* **1954**, *96*, 266−279.

(66) D'yakonov, M. I.; Perel', V. I. Spin orientation of electrons associated with the interband absorption of light in semiconductors. *Sov. Phys.—JETP* **1971**, *33*, 1053−1059.

(67) Tuan, D. V.; Ortmann, F.; Cummings, A. W.; Soriano, D.; Roche, S. Spin dynamics and relaxation in graphene dictated by electron-hole puddles. *Sci. Rep.* **2016**, *6*, 21046.